Modular Origami Approach for Rigid Foldable Steel Load-Bearing Plate Lattices in Arbitrary Sizes

Alfonso Parra Rubio, Andy Dequin, Erik Strand, Neil Gershenfeld

Abstract:

While plate lattices exhibit superior mechanical performance compared to truss lattices at equivalent densities, their fabrication on an engineering scale presents significant challenges, particularly when utilizing structural materials for load-bearing applications. Industry and academia predominantly rely on 3D printing techniques, but encounter limitations in feature size and scalability of energy efficiency for high production rates. In this study, we propose a modular origami design and manufacturing method for creating steel plate lattices at the meso-scale using sheet stock. Rigid-foldable unit cells are cut, folded, and discretely assembled into lattices. Their mechanical performance is simulated and mechanically tested.

1 Introduction

In cellular solids nature found ways to enhance material properties via geometric configurations. A distinctive aspect of these materials is that the geometry of their unit cells influences their properties to the same extent as their constitutive materials [Gibson and Ashby 88]. All cellular materials can be classified in two principal families. If the unit cell is confined to its edges, it is classified as an *open cell*. On the other hand, if the unit cell is contained in both edges and facets, it is identified as a *closed cell* material.

Architected materials are an endeavor to mimic nature's approach to cellular solids. These topology-oriented materials are van interest in current research because they offer methods for producing solids with engineered properties. [Liu 20] demonstrated that given identical relative densities, constituent materials, and topologies, closed-cell architected materials outperform their open-cell counterparts in mechanical properties. [Berger et al. 17]'s pioneering work introduced the term *plate lattice*, showcasing architectures that achieve the Hashin–Shtrikman bound for isotropic stiffness.

However, there exists a gap between the proven properties of plate lattices and their manufacturability. Most existing research on lattice materials has depended on additive manufacturing (AM) techniques, specifically powder bed fusion (PBF), which are capable of producing complex geometries using load bearing materials across various industries [Fidan et al. 24]. Yet, for employing lattices as bulk

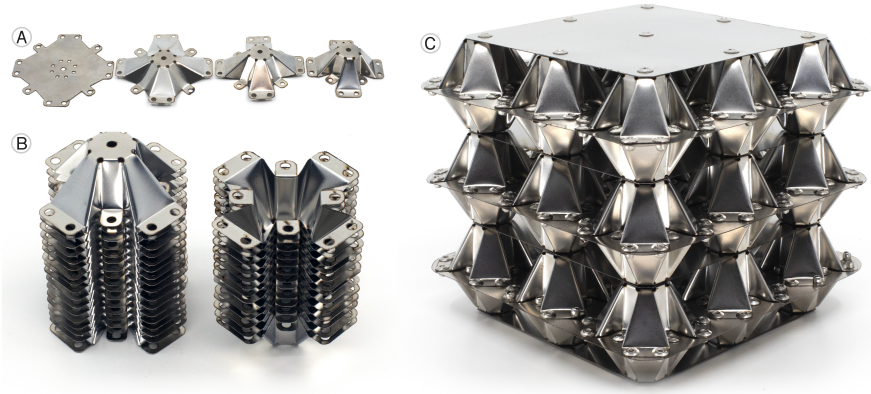

Figure 1: *Metallic Folded Plate Lattice. A) Partial folding states of the unit cells. B) Stacked unit cells. C) 3 by 3 by 3 lattice.*

materials in architectural and engineering applications, AM currently lacks material flexibility, operates at high energy consumption levels relative to production rates [Gutowski et al. 17], and demonstrates a direct correlation between part quality and energy density for structural components [Liu et al. 18].

By contrast, origami methods offer a unique capability since it transform existing materials rather than adding or subtracting. By inherently encoding 3D spatial information within a 2D domain, origami has emerged as a potent design and manufacturing tool for metamaterials and cellular materials. [Cheung et al. 14] revealed highly anisotropic, elastic, and rigid metamaterials based on volumetric tiling of the Miura-ori pattern. [Filipov et al. 15] showed that origami tube-like structures could be hierarchically assembled to create cellular materials with varied mechanical properties. [Miyazawa et al. 21] introduced configurable multicellular origami materials with customized static responses within the same material. Furthermore, [Jamalimehr et al. 22] developed metamaterials with a self-locking unit cell geometry that bears loads along the deployment axis, among many other studies.

These aforementioned research path exploits origami as a design method increasing complexity in the unit cell geometry, which presents significant manufacturing challenges if trying to be manufactured with structural materials.

1.1 Structural Origami Cellular Materials

The most successful attempt of origami engineering that manufacture large scale of folded structural elements from load-bearing materials was in 2005 with the establishment of *Foldcore GmbH*. Work by its founder introduced origami-based open cells for the aerospace industry and related sandwich panels, however these primarily utilized composites as constitutive materials in the form of sandwich panels. [Klett et al. 07] [Klett and Drechsler 11]. In the domain of metallic origami

structures, research by [Li et al. 11] presented folded sandwich construction approaches with open facets, studying various unit cells for energy absorption.

While there maturity in continuum sandwich panel manufacturing is shown, we find a gap that exploits the benefits of folding and assembling for generating larger lattice materials.

This paper proposes an approach for *metallic folded plate lattices*. By employing discretely assembled unit cells we decrease the folding pattern complexity, facilitating a simple manufacturing. By having less creases to fold, we simplify the use of load-bearing materials such as steel to create load bearing plate lattices. We begin by outlining the design process and the analytical method for determining the unit cell geometry. Subsequently, we describe the manufacturing and assembly technique, introduce Periodic Boundary Condition method to search an optimized design, manufacture it, and compare projected performance by quasi-static uniaxial compressive testing.

2 Unit Cell

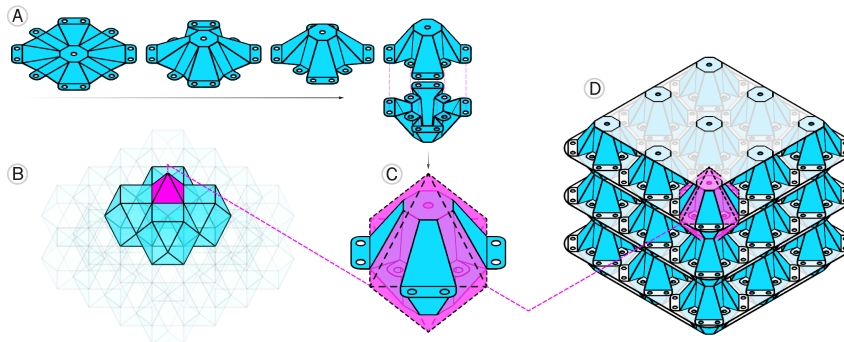

Figure 2: *Plate lattices formed by expanded-truncated rectangular pyramid unit cells. A) Progressive folding from the flat state to the final configuration. B) Semi regular cuboctahedron lattice. Blue: cuboctahedron. Pink: octahedron voids. C) A mirrored expanded-truncated rectangular pyramid realizes the principal planes of the octahedron. D) Vertex connected octahedra form a semi regular lattice.*

The design of this architected plate lattice begins with the topology of the unit cell, which, in this context, is essentially a folded geometry. This section outlines the design process and shows the geometric transformations necessary to satisfy manufacturing and mechanical constraints.

Our work focuses on plate-based cellular materials inspired by semi-regular octahedral lattices. This configuration has gained attention for its capability to be constructed from either a face-connected cuboctahedron unit cell or a vertex-connected octahedron unit cell. This architecture, interpreted as a beam-lattice, satisfies Maxwell's rigidity criteria with the lowest vertex connectivity [Cheung 12].

For our purposes, this implies a reduction in the number of creases that must be folded to form a unit cell.

Figure 2 illustrates our approach to utilizing the vertex-connected octahedron unit cell. We employ what we call an *expanded-truncated rectangular pyramid* as the base shape to form an approximately octahedral unit cell. When these folded geometries are mirrored at their bases, their lateral planes realize the principal facets of an octahedron. In the plane of mirroring, we insert a steel layer where the two rectangular pyramids will be riveted together to form an octahedron and, thereby, restrain its degrees of freedom (DOFs).

The rationale for the truncation and expansion is to satisfy assembly and mechanical constrains. It is important to note that these modifications compromise the lattice's isotropy. As shown in [Parra Rubio et al. 23], the engineering of boundary regions is crucial for discretely assembled cellular materials that will be mechanically joined. By avoiding edge-edge connections and instead providing facet-facet contacts, the assembly process is simplified and can rely on robust and accessible mechanical connections such as riveting, welding or screwing for modular assembly.

The unit cell has 5 DOFs: h, b, w, e, θ_2 and ρ_1. The process we follow and the parameters can be seen in Figures 3 and 4. First, we fold an octahedron-like shape from a flat preform by adding *inside-reverse* folds at each corner. Second, we truncate the top of this geometry as seen in Figure 4 A. Next we take the corner vertex as shown in Figure 3 and calculate the folding angles θ_2 and ρ_1. The final step is to apply the expansion as shown in Figure 4 C.

2.1 Analytical form and DOFs of the expanded-truncated rectangular pyramid

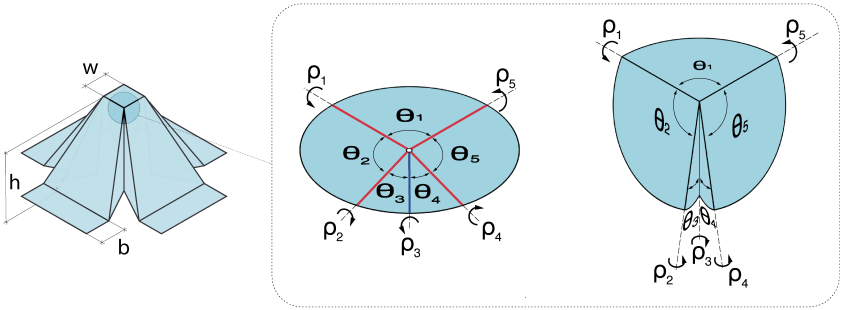

Figure 3: *Unit cell parameters. Left, height (h), width (w) and expanded flaps (b) are denoted. Right, folded and unfolded degree 5 vertex of the unit cell.*

In this section we assume that h, w, b, e, and θ_2 are fixed, since this uniquely determines the geometry of the flat state. Our goal is to describe the geometry

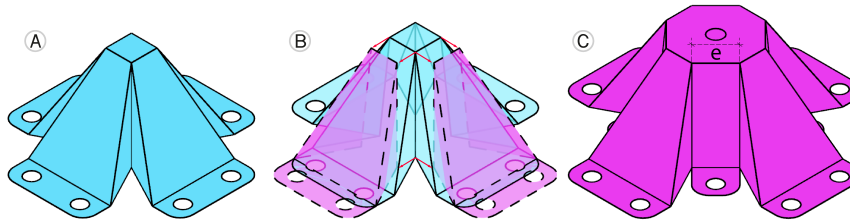

Figure 4: *Expansion process. A) Intermediate cell state used to calculate folding parameters. B) Expansion directions, arrows in red. C) Expanded-truncated rectangular pyramid unit cell.*

of any intermediate or final folded state as a function of ρ_1. In the general case, determining the kinematics of such a rigid origami structure is complicated and usually solved numerically [Tachi 09]. But this design has a number of symmetries that enable a relatively simple analytical solution.

As depicted in Figure 3, each of the four vertices is identical in the flat state. We will require that they evolve identically through all intermediate states. Thus we only need to consider the kinematics of a single vertex.

Within each vertex, by construction $\theta_1 = \pi/2$ radians. We set $\theta_2 = \theta_5$ and $\theta_3 = \theta_4$ to obtain symmetry about crease 3 in the flat state. We ensure that this symmetry is preserved during folding by keeping $\rho_1 = \rho_5$ and $\rho_2 = \rho_4$. With these constraints, the vertex has a single kinematic degree of freedom. The sum of the face angles is 2π, so we may express θ_3 in terms of θ_2.

$$\theta_3 = \frac{3\pi}{4} - \theta_2 \tag{1}$$

Since θ_1 is a right angle, it is convenient to work in a coordinate system centered at the vertex where $\hat{\mathbf{x}}$ lies along crease 5, $\hat{\mathbf{y}}$ along crease 1, and $\hat{\mathbf{z}} = \hat{\mathbf{x}} \times \hat{\mathbf{y}}$. Define vectors $\mathbf{x_1}, \ldots, \mathbf{x_5}$ lying on the five creases, each one with unit magnitude. The positions of $\mathbf{x_1}$ and $\mathbf{x_5}$ are fixed.

$$\mathbf{x_1} = \hat{\mathbf{y}} \tag{2}$$

$$\mathbf{x_5} = \hat{\mathbf{x}} \tag{3}$$

The positions of $\mathbf{x_2}$ and $\mathbf{x_4}$ in the flat state are readily found via rotation about $\hat{\mathbf{z}}$. Their positions in any intermediate state can be found by applying subsequent rotations about $\hat{\mathbf{y}}$ and $\hat{\mathbf{x}}$, respectively.

$$\mathbf{x_2} = -\sin(\theta_2)\cos(\rho_1)\hat{\mathbf{x}} + \cos(\theta_2)\hat{\mathbf{y}} - \sin(\theta_2)\sin(\rho_1)\hat{\mathbf{z}} \tag{4}$$

$$\mathbf{x_4} = \cos(\theta_2)\hat{\mathbf{x}} - \sin(\theta_2)\cos(\rho_1)\hat{\mathbf{y}} - \sin(\theta_2)\sin(\rho_1)\hat{\mathbf{z}} \tag{5}$$

By construction $\mathbf{x_3}$ has a magnitude of one, and by symmetry it lies in the plane characterized by $x = y$. As such, it is convenient to parameterize $\mathbf{x_3}$ with respect to a single degree of freedom a.

$$\mathbf{x_3} = a\hat{\mathbf{x}} + a\hat{\mathbf{y}} - \sqrt{1-2a^2}\hat{\mathbf{z}} \tag{6}$$

The angle between $\mathbf{x_2}$ and $\mathbf{x_3}$ is θ_3. Since these are both unit vectors, we may write this as $\mathbf{x_2} \cdot \mathbf{x_3} = \cos(\theta_3)$. This produces an equation that is quadratic in a. Its two solutions are given below in terms of temporary values u_1, u_2, u_3, and u_4.

$$u_1 = \sin(\theta_2)\sin(\rho_1) \tag{7}$$

$$u_2 = u_1\sqrt{u_1^2 + 2\cos(\theta_2)\sin(\theta_2)(1-\cos(\rho_1))} \tag{8}$$

$$u_3 = (\sin(\theta_2)\cos(\rho_1) - \cos(\theta_2))\cos\left(\theta_2 + \frac{\pi}{4}\right) \tag{9}$$

$$u_4 = 1 + u_1^2 - 2\cos(\theta_2)\sin(\theta_2)\cos(\rho_1) \tag{10}$$

$$a = \frac{(u_3 \pm u_2)}{u_4} \tag{11}$$

For all physically realizable configurations both roots are real, indicating that faces three and four can be folded toward the inside or outside of the pyramid. We intend to fold these faces inward, so we select the maximum of the two solutions. Since u_1, u_2, u_3, and u_4 depend only on θ_2 and ρ_1, this gives us a closed form solution for x_3.

Given $x_1, \ldots, x_5$, it is easy to compute the crease angles. The cross product of two adjacent crease vectors gives the normal vector of the face they enclose. Each crease angle can be computed as the angle between the normal vectors of the crease's two adjacent faces.

3 Manufacturing

This paper introduces a simple and scalable manufacturing method for fabricating metallic plate lattices via progressive folding and modular assembly. In our study, we employ stainless steel sheet stock with a thickness of 180 microns.

The process of folding metallic sheets necessitates overcoming plastic deformation. Creases, form local areas of high strain, which necessitates the selection of a material with high toughness with a high ultimate stress. However, the inherent trade-off between toughness and strength in materials [Ritchie 11] requires a compromise. Martensitic steels are ideal for their strength, whereas austenitic steel offers better formability. In this paper we use cold worked austenitic 301 stainless steel, as this material is widely available, recyclable and economically affordable.

3.1 Unit cell folding

After calculating the unit cell and all its intermediate folding states, we progress to cutting the stainless steel sheets in its unfolded configuration. We employ the FabLight 3000 laser cutter equipped with a 3kW laser. To mitigate local malformations

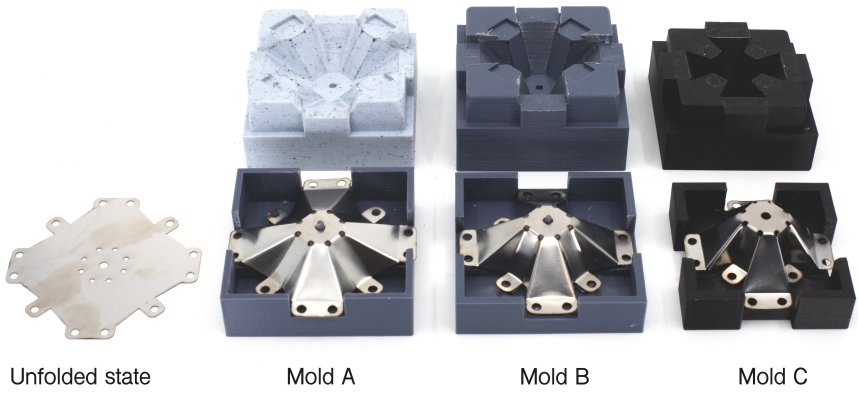

Figure 5: *Manufacturing molds and partially folded unit cells.*

at the vertices of the truncated facet, Figure 5 shows how we introduce small holes at each vertex, where multiple creasing lines converge.

The next step involves progressive molding. We create three distinct molds, each corresponding to a different folding state of the unit cell. Mold A corresponds to a 20% total fold, mold B to 60%, and mold C to 105%. All molds are designed to serve as press forming molds with concave and convex shapes for the corresponding partial folding configurations. We 3D print each mold using PLA. A 2-ton manual arbor press is utilized to shape the metal into the desired mold forms.

Mold A's role is to imprint the crease map onto the stainless steel preform. Mountains and valleys are precisely stamped onto the material to guarantee successful assembly and overall lattice precision. We achieve repetitive and accurate creasing by employing pins to prevent translations and aligning features to avoid undesired rotations.

Once the creasing map is imprinted, we use Mold B to apply a significantly larger strain on the creases to prepare it for the final mold.

Mold C intentionally overfolds the cell, taking into account springback phenomenon. The springback angle has been empirically calculated.

3.2 Discrete lattice assembly

We introduce a modular approach for assembling pre-folded unit cells into lattices. Most origami tessellations used to create cellular structures are based on parallel origami consisting of multiple vertices from which creases emerge to connect other vertices. Materials like paper, which easily deform out of plane, compliantly deform to accommodate the folding process, achieving the desired final shape. However, folding monolithic tessellations from load-bearing materials that resist out-of-plane deformation poses substantial challenges. Our method involves discretizing the tessellation and folding individual unit cells for subsequent assembly. This technique facilitates the manufacturing of metallic plate lattices in an

arbitrary array of n by m by i unit cells. Additionally, the geometry streamlines assembly since all connections are aligned along the Z-axis, presenting significant automation potential through gantry systems [Jenett 20] or robot swarms [Gregg et al. 24] [Jenett et al. 19]. For this iteration we will use stainless steel blind rivets as the mechanical connectors.

Figure 6 illustrates the assembly strategy for a lattice composed of 3x3x3 unit cells. The construction progresses from the bottom up, requiring coordination only with elements in the immediately adjacent layer. This 2.5D assembly method alternates between two modes, ensuring row-by-row assembly by coordinating between the upper and lower layers. The first mode involves aligning the truncated face with its corresponding mirror cell, shown in Figure 6 step 1 for the coordination motion and step 2 for the outcome. The second mode involves the coordination and assembly of expanded base flaps, enclosing a base plate, demonstrated in step 3. This procedure is repeated until the desired structure is achieved.

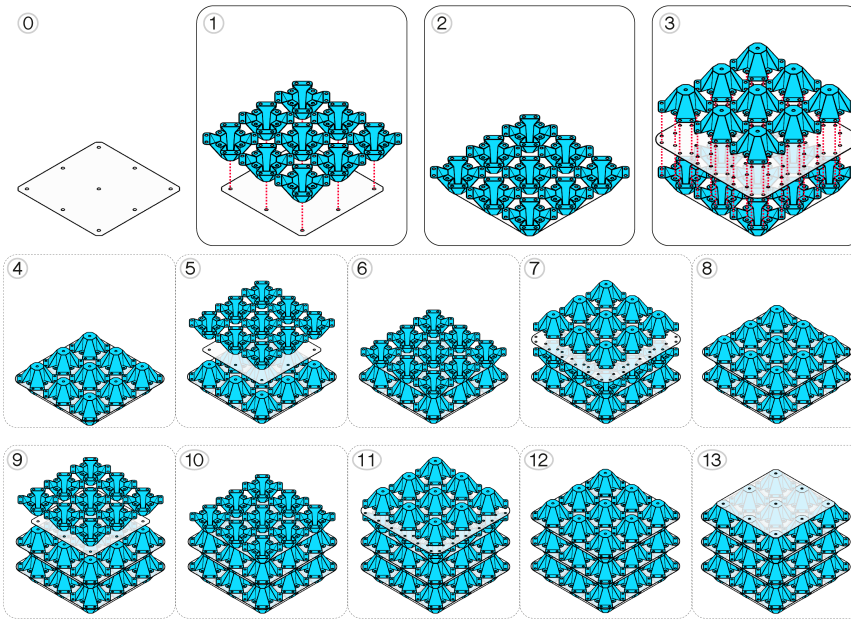

Figure 6: *Assembly process for a plate lattice size 3 by 3 by 3.*

4 Modeling

To analyze the mechanical response of the proposed plate lattices under uniaxial compression, we conducted nonlinear finite element simulations with ABAQUS CAE. This involved a stochastic search across numerous unit cell candidates to select one optimized for performance and manufacturability, followed by detailed

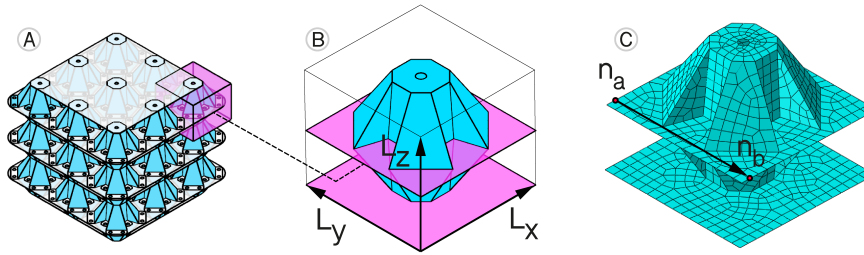

Figure 7: *Periodic Boundary Conditions diagram. A) RVE selected. B) Lattice vector components. C) Meshed cell with n_a and n_b being paired nodes as they satisfy equation 12.*

simulation of a compression test on a 3x3x3 lattice.

4.1 Periodic Boundary Conditions

Simulating plate lattices becomes computationally intensive with increasing mesh size, especially in lattices with numerous unit cells. Lattices with fewer elements face boundary node dominance, while those with extensive unit cells achieve optimal performance through internal node predominance.

To simulate infinitely large cellular solids with minimal computational cost, we employ Periodic Boundary Conditions (PBC). This approach involves selecting a Representative Volume Element (RVE)—our unit cell—and adjusting the DOFs of boundary nodes and the constitutive equation, significantly reducing element count, convergence time, and computational power.

As the RVE is spatially periodic, Figure 7 illustrates the definition of **RVE** as the bounding box of our unit cell, delineated by three lattice vectors $\mathbf{LV_x}$, $\mathbf{LV_y}$, and $\mathbf{LV_z}$.

The unit cell is meshed with symmetric seeding across the XY, XZ, and YZ planes. Nodes are selected if they satisfy the following equation:

$$n_b - n_a = n_1 LV_x + n_2 LV_y + n_3 LV_z \tag{12}$$

where n_b and n_a are the node coordinates and n1, n2 an n3 the three components of any possible linear combination of the 3D Lattice Vector:

$$\begin{bmatrix} n_1 \\ n_2 \\ n_3 \end{bmatrix} = \begin{bmatrix} 1 \\ 0 \\ 0 \end{bmatrix} or \begin{bmatrix} 0 \\ 1 \\ 0 \end{bmatrix} or \begin{bmatrix} 0 \\ 0 \\ 1 \end{bmatrix} or \begin{bmatrix} 1 \\ 1 \\ 0 \end{bmatrix} or \begin{bmatrix} 0 \\ 1 \\ 1 \end{bmatrix} or \begin{bmatrix} 1 \\ 0 \\ 1 \end{bmatrix} or \begin{bmatrix} 1 \\ 1 \\ 1 \end{bmatrix} \tag{13}$$

We now pair their displacements with the following equation:

$$\mathbf{u_b} - \mathbf{u_a} = \mathbf{H}(X_b - X_a) \tag{14}$$

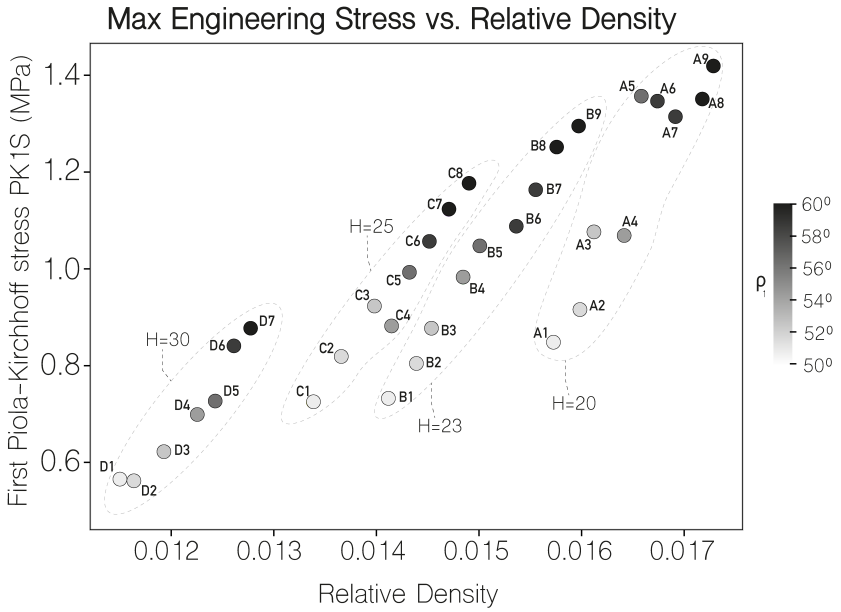

Figure 8: *Simulations for Ultimate Compressive Strength vs. Relative Density for all samples.*

where **H** is the displacement gradient matrix and X_a and X_b are the coordinate of the selected nodes at the undeformed mesh state. The matrix X can be now designed with three virtual nodes that will impose a macroscopic deformation. In our case, as we want s_z,a constant strain value that correspond to uniaxial compression in the Z-axis:

$$\mathbf{H} = \begin{bmatrix} u_{x,VirtualNode1} u_{y,VirtualNode1} u_{z,VirtualNode1} \\ u_{x,VirtualNode2} u_{y,VirtualNode2} u_{z,VirtualNode2} \\ u_{x,VirtualNode3} u_{y,VirtualNode3} u_{z,VirtualNode3} \end{bmatrix} = \begin{bmatrix} 0\,0\,0 \\ 0\,0\,0 \\ 0\,0\,s_z \end{bmatrix} \tag{15}$$

We implement PBC using Abaqus scripting and run a batch of simulations to obtain the unit cell stress response to the strain. We run simulations for different heights, different ρ_1 values and same $\theta 2$.

Figures 9 and 8 present simulation results employing Periodic Boundary Conditions (PBC) on steel folded unit cells with a thickness of 180 microns. The samples are labeled with part numbers, which are detailed in Table 1. The simulations account for the elastoplastic behavior of stainless steel 301, parameters of which were derived from dogbone tests conducted using an Instron 5985. We mesh the geometry using SR4 elements with 5 Gauss integration points. The unit cell was subjected to a strain of 0.1, following which we processed the results to calculate the stress and stiffness values of the unit cell. Notably, instead of calculating Cauchy stresses,

Table 1: *Part names and unit cell parameters.*

Part Number	Height (mm)	ρ_1(deg)	θ_2(deg)
A1	20	51	106
A2	20	53	106
A3	20	54	106
A4	20	56	106
A5	20	57	106
A6	20	58	106
A7	20	59	106
A8	20	60	106
A9	20	61	106
B1	23	51	106
B2	23	53	106
B3	23	54	106
B4	23	56	106
B5	23	57	106
B6	23	59	106
B7	23	60	106
B8	23	61	106
B9	23	62	106
C1	25	52	106
C2	25	54	106
C3	25	56	106
C4	25	57	106
C5	25	58	106
C6	25	59	106
C7	25	60	106
C8	25	61	106
D1	30	51	106
D2	30	52	106
D3	30	54	106
D4	30	56	106
D5	30	57	106
D6	30	58	106
D7	30	59	106
D8	30	60	106

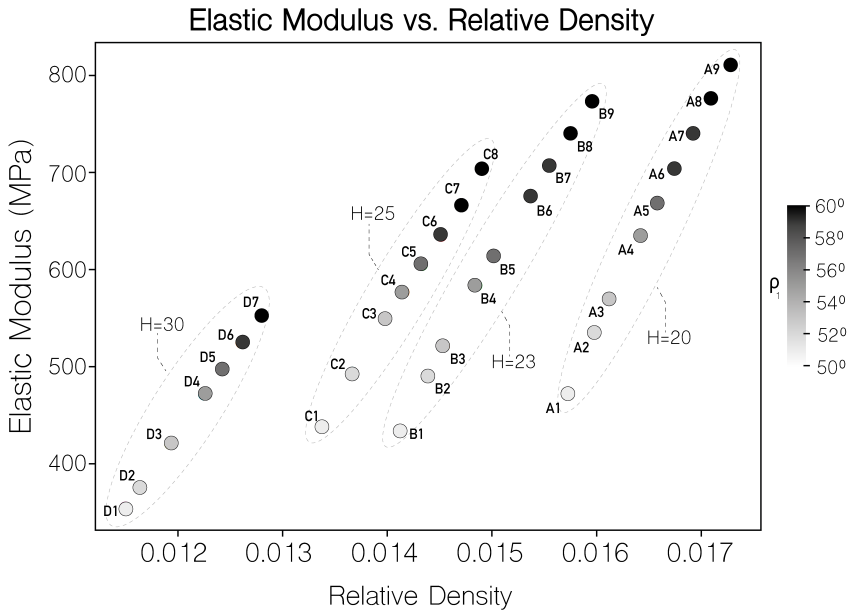

Figure 9: *Simulations for Elastic Modulus vs. Relative Density.*

we obtain the first Piola-Kirchhoff stresses, as our analysis is based on the initial volume state.

We choose to manufacture a lattice with the sample A8, as it combines both good performance in the simulations and manufacturability. Performance-wise we see that it maximizes stresses and stiffness. This model is more easily manufactured as it tiles well in the unfolded state, making efficient use of the sheet feedstock and the folding angles are suitable for a good formability.

4.2 Modelling of a 3x3x3 lattice

We simulate a 3x3x3 lattice using sample 8. The unit cell parameters can be seen in Table 1. The simulation parameters are the same as the one defined in the PBC subsection, but in this case we will uniaxially compress the lattice by 20 mm.

5 Results

We fabricated a 3x3x3 lattice using the selected A8 topology. The cellular structure weighs 560 grams, measuring 150mm x 150mm x 123mm, resulting in a relative density of 0.023, exceeding the anticipated 0.019. This additional weight is attributed to the parasitic mass of steel rivets utilized in assembly, which was not accounted for in the performance projections of the unit cell. Figure 10 depicts

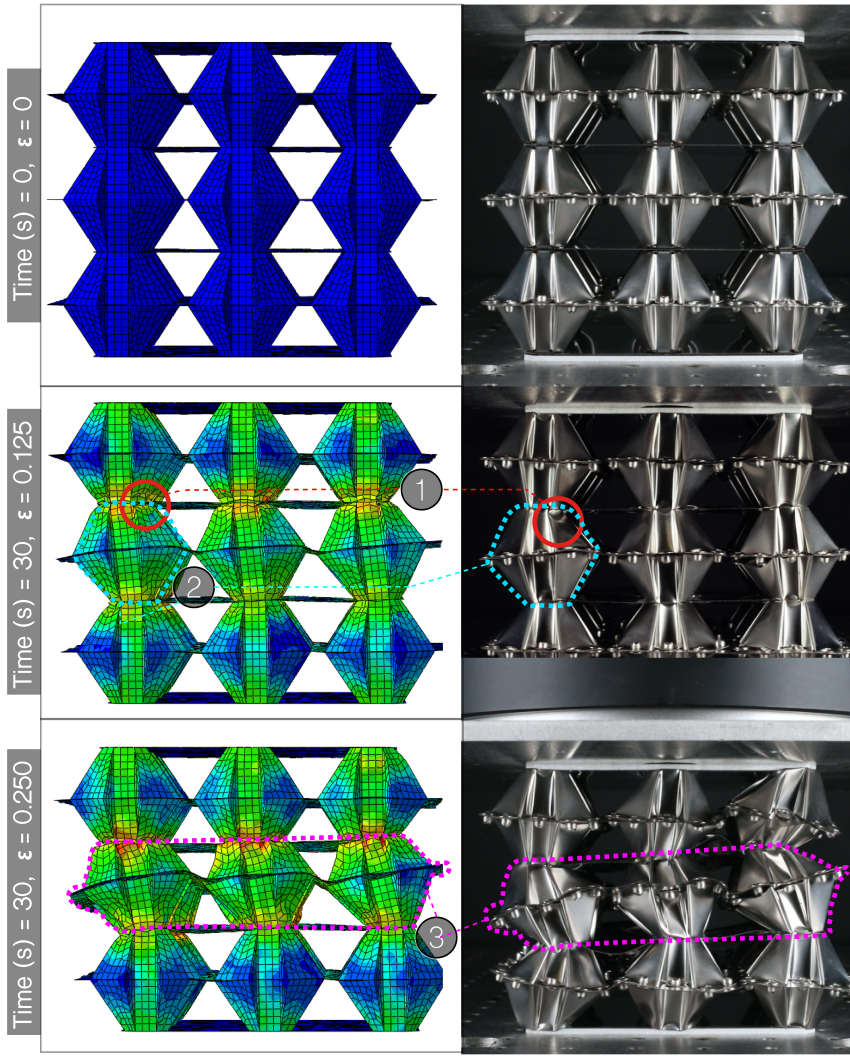

Figure 10: *Qualitative comparison for simulated (left) and testing (right). 1) Local shell buckling. 2) Unit cell shearing. 3) Shear propagation.*

the steel lattice subjected to uniaxial compression testing, using an Instron 5985, conducted at a strain rate of 10 mm/min.

Figure 11 compares the mechanical responses of both the simulated and actual lattices. The simulation indicates a stiffer response under load, with a maximum load of 37kN before plastic deformation begins. Conversely, the test sample displayed a slightly less stiff behavior but closely matched maximum load value around 33kN. This stress level corresponds to 1.47 MPa, closely aligning with the

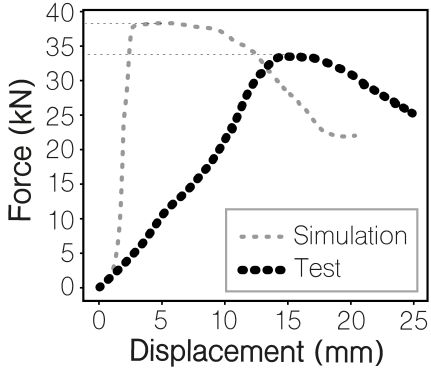

Figure 11: *Force-Displacement results for the simulated lattice and the tested lattice. While we see accurate predicted stress values, the simulated lattice shows to be stiffer as it dont count for manufacturing feature as folding radii and discrete connections.*

projected 1.37 MPa from PBC simulations for that unit cell.

While the stress projections and simulations were accurate, two factors may explain the observed discrepancy in stiffness: First, our model does not account for radii in the folds, assuming them to be infinitely sharp. Besides, some dome curvature was noted in the manufactured truncated facets, potentially increasing the unit cell's compliance. Second, the effect of the rivet assembly was not simulated, although no rivets were observed to fail by shear during compression testing.

6 Conclusions

We introduced a modular origami design and manufacturing approach for producing meso-scale steel plate lattices. We rely on progressive folding through press forming molding, a base technology that can be scaled to high throughput while demanding less energy consumption than competing processes. We developed a method to evaluate mechanical responses of parametrized topologies, fabricated the optimal configuration, and conducted mechanical testing. This method presents a straightforward avenue for the automated production of meso-scale metallic lattices for structural applications at a considerably lower cost. Future reseach work will focus on refining connection strategies, investigating welded assemblies, exploring alternative base geometries (e.g., triangular truncated pyramids), and experimenting with different constituent materials. Regarding industrial utilization and commercialization, the architected structures presented in this paper demonstrate promising size scalability owing to their custom relative density. This make them suitable candidates for on-site deployed structures in aerospace and architecture. Additionally, their exceptional energy absorption characteristics and strength-to-cost ratio position them as excellent candidates for applications within the automotive sector. Besides, further research into thermal and acoustic insulation properties can be explored utilizing this geometric framework.

7 Acknowledgements

This work was supported by the Center for Bits and Atoms Research Consortia. The authors would like to express their gratitude to: Katia Bertoldi, Connor McCann, and David Farrell for teaching nonlinear Finite Element Theory and support. The Structural Origami Gathering for their ongoing intellectual encouragement and support.

References

[Berger et al. 17] J. Berger, Wadley, H., and R. McMeeking. "Mechanical metamaterials at the theoretical limit of isotropic elastic stiffness." *Nature*.

[Cheung et al. 14] Kenneth C. Cheung, Tomohiro Tachi, Sam Calisch, and Koryo Miura. "Origami interleaved tube cellular materials." *Smart Materials and Structures*.

[Cheung 12] Kenneth C. Cheung. "Digital Cellular Solids: reconfigurable composite materials." Ph.D. thesis, Massachusetts Institute of Technology, 2012.

[Fidan et al. 24] Fidan, Ismail, Vivekan, Naikwadi, Suhas Alkunte, Roshan Mishra, and Khalid Tantawi. "Energy Efficiency in Additive Manufacturing: Condensed Review." *Technologies*.

[Filipov et al. 15] Evgueni T. Filipov, Tomohiro Tachi, , and Glaucio H. Paulino. "Origami tubes assembled into stiff , yet reconfigurablestructures, metamaterials." *PNAS*.

[Gibson and Ashby 88] Lorna J. Gibson and Michael F. Ashby. *Cellular Solids and Structure and Properties*. Cambridge University Press, 1988.

[Gregg et al. 24] Christine E. Gregg, Damiana Catanoso, Olivia Irene B. Formoso, Irina Kostitsyna, Megan E. Ochalek, Taiwo J. Olatunde, In Won Park, Frank M. Sebastianelli, Elizabeth M. Taylor, Greenfield T. Trinh, and Kenneth C. Cheung. "Ultralight, strong, and self-reprogrammable mechanical metamaterials." *Science Robotics*.

[Gutowski et al. 17] Timothy Gutowski, Sheng Jiang, Daniel Cooper, Gero Corman, and Jan-Anders; Schudeleit Timo; Wegener Konrad; Sabelle Matias; Ramos-Grez Jorge; Sekulic Dusan P Hausmann, Michael; Manson. "Note on the Rate and Energy Efficiency Limits for Additive Manufacturing." *Journal of Industrial Ecology*.

[Jamalimehr et al. 22] Amin Jamalimehr, Morad Mirzajanzadeh, Abdolhamid Akbarzadeh, and Damiano Pasini. "Rigidly flat-foldable class of lockable origami-inspired metamaterials with topological stiff states." *Nature Communications*.

[Jenett et al. 19] Benjamin Jenett, Amira Abdel-Rahman, Kenneth Cheung, and Neil Gershenfeld. "Material–Robot System for Assembly of Discrete Cellular Structures." *IEEE Robotics and Automation Letters*.

[Jenett 20] Ben Jenett. "Discrete Mechanical Metamaterials." Ph.D. thesis, MIT, 2020.

[Klett and Drechsler 11] Yves Klett and Klaus Drechsler. "Designing Technical Tessellations." *Origami 5: International Meeting of Origami Science, Mathematics and Education.*

[Klett et al. 07] Y Klett, K Drechsler, M Kolax, H Wentzel, and R Kehrle. "Design of multifunctional folded core structures for aerospace sandwich applications." *CEAS European Air and Space Conference*.

[Li et al. 11] Zhejian Li, Wensu Chen, and Hong Hao. "Quasi-static-crushing-behaviours-of-folded-open-top-truncated-pyramid-structures-with-interconnected-side-walls.pdf." *Origami 7: International Meeting of Origami Science, Mathematics and Education.*

[Liu et al. 18] Z.Y. Liu, C. Li, X.Y. Fang, and Y.B. Guo. "Energy Consumption in Additive Manufacturing of Metal Parts." *Procedia Manufacturing*.

[Liu 20] Y. Liu. "Mechanical properties of a new type of plate–lattice structures." *Journal of Mechanical Sciences*.

[Miyazawa et al. 21] Yasuhiro Miyazawa, Hiromi Yasuda, Hyungkyu Kim, James H. Lynch, Kosei Tsujikawa, Takahiro Kunimine, and Jordan R. Raney Jinkyu Yang. "Heterogeneous origami-architected materials with variable stiffness." *Communications Materials*.

[Parra Rubio et al. 23] Alfonso Parra Rubio, Klara Mundilova, David Preiss, Erik Demaine, and Neil Gershenfeld . "Kirigami Corrugations: Strong and Modular and and Programmable Plate Lattices." *Proceedings of the ASME 2023 International Design Engineering Technical Conferences and Computers and Information in Engineering Conference. Volume 8: 47th Mechanisms and Robotics Conference (MR).*

[Ritchie 11] R. Ritchie. "The conflicts between strength and toughness." *Nature*.

[Tachi 09] Tomohiro Tachi. "Simulation of Rigid Origami." *Origami 4: Fourth International Meeting of Origami Science, Mathematics, and Education* 4. doi:10.1201/b10653-20.

Alfonso Parra Rubio
Massachusetts Institute of Technology, Center for Bits and Atoms, e-mail: aprubio@mit.edu

Andy Dequin
Massachusetts Institute of Technology, Center for Bits and Atoms, e-mail: dequin@mit.edu

Erik Strand
Massachusetts Institute of Technology, Center for Bits and Atoms, e-mail: strand@cba.mit.edu

Neil Gershenfeld
Massachusetts Institute of Technology, Center for Bits and Atoms, e-mail: gersh@cba.mit.edu